MORPHOLOGICAL SIGNAL ADAPTIVE MEDIAN FILTER FOR NOISE REMOVAL

Sofia Tsekeridou *Constantine Kotropoulos* *Ioannis Pitas*
Department of Informatics
Aristotle University of Thessaloniki
Box 451, 54006 Thessaloniki, GREECE.
E-mail: pitas@zeus.csd.auth.gr

ABSTRACT

A novel extension of the classical signal-adaptive median filter (SAM) is proposed in this paper. It is the so-called morphological signal-adaptive median filter ($MSAM$). Two modifications are introduced in the SAM filter aiming at: (1) enhancing SAM impulse detection mechanism so that it detects not only impulses of a constant amplitude but randomly-valued impulses as well, (2) employing an anisotropic window adaptation based on binary morphological erosions/dilations with predefined structuring sets. Performance results are reported by evaluating both objective criteria (e.g. SNR, MAE) and subjective criteria (e.g. the perceived quality of the filtered images). The proposed $MSAM$ filter outperforms the classical SAM filter in all cases.

1. INTRODUCTION

The corruption of images by noise is a frequently encountered problem in many image processing tasks. The observed noise can be modeled either as additive white, impulsive, signal-dependent or a combination of them [1]. Therefore, the need emerges for implementing smoothing techniques that are able to treat different kinds of noise. Furthermore, a noise-free version of the corrupted image required by adaptive filtering algorithms during the training procedure is not always available. Moreover, it is well known that the main objectives of image filtering algorithms are: (a) the suppression of noise in homogeneous regions, (b) the preservation of edges and (c) the removal of impulses of constant as well as of random value [1, 2]. A class of filters that fulfills these requirements is the so called *signal-adaptive filters*. Signal-adaptive median (SAM) is a paradigm of this class [1]. Other signal-adaptive filters are proposed in [3, 4].

A novel extension of the classical signal-adaptive median filter (SAM) is proposed in this paper. It is the so-called *morphological signal-adaptive median filter ($MSAM$)*. This filter performs well on many kinds of noise. It does not require a priori knowledge of a noise-free image, but only of certain noise characteristics, which can easily be estimated. It adapts its behaviour based on a local SNR measure achieving thus edge preservation and noise smoothing in homogeneous regions. It smooths the impulsive noise as well.

2. MORPHOLOGICAL SIGNAL ADAPTIVE MEDIAN FILTER

To begin with, let us describe the framework for signal-adaptive filters. Let σ_n^2 denote the noise variance that is known or has been estimated beforehand. Moreover, in the case of impulsive noise let p_p be the percentage of positive impulses (i.e., $S_{max} = 255$), and p_n be the percentage of negative impulses (i.e., $S_{min} = 0$). Thus, the noisy image pixel values $x(k,l)$ are determined by the model:

$$x(k,l) = \begin{cases} S_{min} & \text{with prob. } p_n \\ S_{max} & \text{with prob. } p_p \\ x(k,l) & \text{with prob. } 1-(p_p+p_n) \end{cases} \quad (1)$$

where $x(k,l)$ is an image pixel corrupted possibly by additive white or signal-dependent noise. An image can be considered as a sum of two components: $x(k,l) = x_L(k,l) + x_H(k,l)$, i.e., a low-frequency component $x_L(k,l)$ which is dominant in homogeneous regions, and a high frequency one $x_H(k,l)$ observed in edges. The output of the $MSAM$ filter is expressed as in the classical SAM filter, i.e.,

$$y(k,l) = \tilde{x}_M(k,l) + b(k,l)[x(k,l) - \tilde{x}_M(k,l)]. \quad (2)$$

$\tilde{x}_M(k,l)$ is the modified median, i.e., the median of the pixels that remain after the removal of impulses from the local window. $b(k,l)$ is a weighting coefficient that is used to adapt the window size according to whether a flat region or an edge has been met. It is evident that total noise suppression is achieved in homogeneous regions, because a large window is employed due to $b(k,l)$ being close to 0. Edges are also preserved well, because a small window size is used due to $b(k,l)$ being close to 1 in this case. The window increment/decrement procedure is explained below. Two major modifications in the classical SAM filter [1] are introduced in the proposed $MSAM$ filter: **(1)** $MSAM$ employs the morphological operations of dilation and erosion with certain predefined structuring elements (SEs) in order to vary the window size anisotropically with respect to the local image content. **(2)** $MSAM$ employs two impulse detectors: one for constant impulses (either positive or negative) and another for randomly-valued impulses. Impulse detection is done only in the initial window of dimensions 3×3. Subsequently, the several steps of the algorithm are presented.

1. Constant value impulse detection [1]: The filter performs detection of constant value

impulses in an initial window of dimensions 3×3 by using a signal-dependent threshold $\tau_n(k,l)$ for negative impulses given by:

$$\tau_n(k,l) = c[S_{min} - \tilde{x}_M(k,l)] \leq 0 \qquad (3)$$

and another one for positive impulses defined by:

$$\tau_p(k,l) = c[S_{max} - \tilde{x}_M(k,l)] \geq 0 \qquad (4)$$

where c is a constant equal to 5/6. If $[x(k,l) - \tilde{x}_M(k,l)] < \tau_n$ then $x(k,l)$ is detected as a negative impulse. Similarly, if $[x(k,l) - \tilde{x}_M(k,l)] > \tau_p$ then $x(k,l)$ is detected as a positive impulse.

2. Randomly-valued impulse detection: Motivated by the randomly-valued impulse detection mechanisms developed in [4, 5], two additional thresholds are introduced in the classical SAM filter. They are defined as follows:

$$h_1(k,l) = x_{max} - x_{min2} \qquad (5)$$
$$h_2(k,l) = x_{max2} - x_{min} \qquad (6)$$

where x_{min} is the minimum value pixel, x_{min2} is the second minimum value pixel, x_{max} is the maximum value pixel and x_{max2} is the second maximum value pixel in the initial window. If $|x(k,l) - \tilde{x}_M(k,l)|$ is greater than any of the thresholds h_1 or h_2, then $x(k,l)$ is of very small or of very large value with respect to its neighbouring pixels and most possibly is a randomly-valued impulse. If the current pixel is an impulse, either constant or randomly-valued, it is excluded from the estimation of the median at the current and at any future window centered at (k,l) yielding the modified median employed in (2).

3. Calculation of the weighting coefficient $b(k,l)$. This coefficient is given by the expression [1]:

$$b(k,l) = \begin{cases} 0, & \text{if } \alpha\sigma_n^2 \geq \hat{\sigma}_x^2 \\ (1 - \alpha\frac{\sigma_n^2}{\hat{\sigma}_x^2})^\beta, & \text{otherwise.} \end{cases} \qquad (7)$$

$\hat{\sigma}_x^2$ denotes the image variance estimated from the local "windowed" histogram by excluding the current pixel if it is detected as an impulse [1]. α and β are appropriately chosen parameters in the interval [0, 1]. The parameter α controls the threshold on the local signal to noise ratio up to which the high-frequency components are entirely suppressed. The parameter β controls the suppression of noise close to edges.

4. Decision whether the current pixel belongs to a homogeneous region or to an edge. The weighting factor $b(k,l)$ calculated in Step 3 is compared to a predefined threshold b_t. If it is smaller than b_t, then the current pixel is assumed to belong to a homogeneous region. Otherwise, the current pixel belongs to an edge. The threshold b_t lies in the interval [0, 1]. Its selection is accomplished in accordance with the degree of corruption and the nature of noise. For highly corrupted images, its value is lower than 0.5. If the image is corrupted by pure Gaussian noise of relatively medium variance, the threshold lies in the range [0.65, 0.85]. A reliable method for the choice of the threshold b_t is described in [1]. Methods employing local statistics have been reported in [3].

5. Novel window adaptation procedure. The proposed $MSAM$ differs from the SAM filter in the window adaptation procedure used. SAM employs isotropic filter windows of dimensions 3×3 up to 11×11. In contrast to SAM, an anisotropic window adaptation procedure is proposed based on mathematical morphology erosions/ dilations with predefined structuring elements. Four structuring elements are employed, namely, B_1, B_2, B_3 and B_4 and their symmetric ones B_1^s, B_2^s, B_3^s and B_4^s illustrated in Figure 1a. They are divided in even-angle SEs (B_1, B_2, B_1^s, B_2^s) and in odd-angle SEs (B_3, B_4, B_3^s, B_4^s). The window increment is performed by a dilation operation $W \oplus B_i$, where W denotes the current filter window. The "direction" of increment depends on the choice of B_i. The result of the window growing $W \oplus B_i$ for an original 3×3 window size W is shown in Figure 1b. The thin dots belong to the original window W while the bold dots denote the new pixels that have been appended to W forming thus the new (larger) window. In an analogous fashion, the window decrement is performed by an erosion operation $W \ominus B_i$. This is demonstrated in Figure 1c for B_1, B_1^s, B_2, B_2^s. It is worth noting that only these SEs are used for reducing the window size. The procedure of the window adaptation begins with a 3×3 square window and checks whether the central pixel belongs to an edge.

I. If it does not belong to an edge:

(a) An attempt is made to increase the window size by using the odd-angle SEs.
(i) If an edge is **"hit"** (e.g. $b(k,l) > b_t$) any odd-angle SE employed is excluded and the even-angle SEs that compose it are tested for possible window increment. For example, if B_4 is excluded, B_1 and B_2 are tested for possible window increment. This means that the sides of the mask are also separately checked expecting that an edge is possibly met at one side only. By doing so, maximal window increment is achieved.
(ii) If an edge is **not** met, then the odd-angle SE is used to increase the window size. The corresponding even-angle SEs are then excluded.

(b) In the next step, the odd-angle SEs, that have not been excluded in a previous step, are tested again. In the above-described example, B_3, B_3^s and B_4^s remain to be tested. In other words, if it is known from a previous step that a window side meets an edge, this side is not considered again.

(c) The procedure continues until all the odd-angle and all the even-angle SEs are excluded or until at least one side reaches a maximal size (e.g., 11).

II. If the pixel belongs to an edge, the goal is to expand the mask in the neighbouring regions that are homogeneous. That is, the current pixel is labeled as a border pixel and the window increment is done towards the side of the edge where the pixel belongs to. To do so, the opposite side of the edge must be found and the incre-

ment of the filter window towards that direction must be prohibited. This is done as follows. The average value of the pixels on each of the four sides of a window of dimensions 3×3 is derived and the absolute difference between these average values and the current pixel is calculated. The side that corresponds to the greater difference is removed. The difference is a measure of deviation of the side pixels from the current one. The side that deviates the most is possibly the side that should be removed. The decrement of the initial window size is achieved by the operation of erosion with one of the SEs B_1, B_1^s, B_2, B_2^s. Subsequently, the window increases towards the remaining sides in the way described above by using appropriate SEs. For example, if erosion with B_1 were performed, B_1, B_2, B_2^s, B_3, B_4^s would be used to increase further the window.

Finally, if the current pixel is detected as an impulse, the factor $b(k,l)$ is set to 0 (thus allowing maximum filtering).

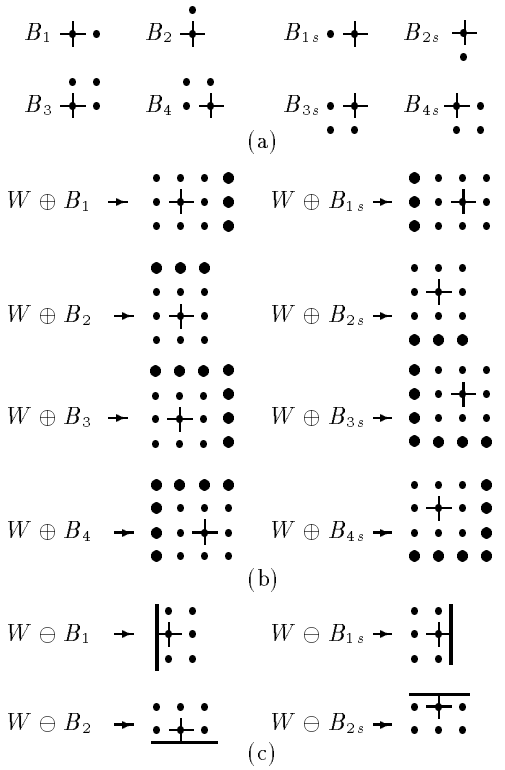

Figure 1. (a) Structuring Sets. (b) Window Increment using Dilation. (c) Window Decrement using Erosion.

3. SIMULATION RESULTS AND CONCLUSIONS

The noise-free image "Airfield" has been corrupted by adding white i.i.d. noise obeying the pdf of a Gaussian mixture given by:

$$n \sim (1-\lambda)N(0,\sigma_\nu) + \lambda N(0,\frac{\sigma_\nu}{\lambda}) \qquad (8)$$

with mean value $E(n)$ close to 0, and variance $\sigma_n^2 = \sigma_\nu^2(1-\lambda+1/\lambda)$ [6]. The contamination factor λ, along with the initial standard deviation σ_ν, determine the degree of corruption. The result of this noise corruption process is a mixture of Gaussian and impulsive noise of varying characteristics according to the value of both λ and σ_ν. It is worth noting that the special case of pure constant value impulsive noise is additionally examined in order to test the robustness of the proposed filter in this kind of noise as well.

Two objective criteria have been evaluated for each pair of noisy and filtered images, namely the SNR and the MAE, defined by:

$$\hat{SNR} = 10\log_{10}\frac{\hat{\sigma}_d^2}{\hat{\sigma}_n^2} \qquad (9)$$

$$\hat{MAE} = \frac{1}{NM}\sum_{k=1}^{N}\sum_{l=1}^{M}|n(k,l)| \qquad (10)$$

where $n(k,l) = y(k,l) - d(k,l)$ is the output noise, $d(k,l)$ is the noise-free image and $y(k,l)$ denotes the filtered image. $\hat{\sigma}_d^2$ is the variance of the noise-free image and $\hat{\sigma}_n^2$ is the variance of the output noise. N, M correspond to the number of image rows and columns, respectively.

A wide range of noise sequences has been added to the noise-free image "Airfield" of dimensions 512×512. Part of the original image is shown in Figure 2a. Due to lack of space, three cases are only reported. First, "Airfield" is corrupted by noise having a contaminated Gaussian distribution (8) with values for $\lambda = 0.1$ and $\sigma_\nu^2 \simeq 586.5$. This leads to a high corruption of the original image by both impulsive and Gaussian noise. Part of the corrupted image is shown in Figure 2b. Second, λ is chosen to be equal

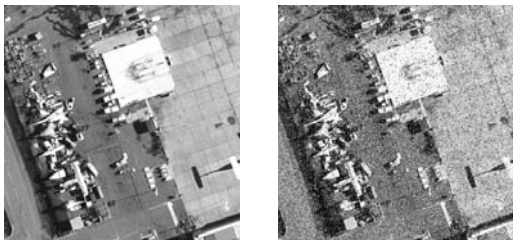

(a) (b)

Figure 2. (a) Part of the noise-free image: Airfield. (b) Part of the original image corrupted by both impulsive and gaussian noise.

to 1.0 which implies that only pure Gaussian noise is present in the noisy image. A value close to 474.0 has also been used for σ_ν^2. Finally, an impulsive noise of 10% positive and 10% negative constant value impulses has been added to "Airfield" to test the robustness of the proposed algorithm for pure impulsive noise. The simulation results for the three cases are listed in Table 1. For comparison purposes, results obtained by using the SAM and the median filter of dimensions 3×3 are also included in Table 1. To facilitate the comparison between the filtered images only a part of all images is demonstrated. Figure 3a shows the output of the morphological SAM filter corresponding to the image part that is examined. The output of the classical SAM filter and the median filter of dimensions 3×3 is shown in Figures 3b and 3c, respectively. The inspection of Table 1 manifests that

(a) (b) (c)

Figure 3. The same part of the noisy image under study processed by: (a) the morphological *SAM* filter, (b) the *SAM* filter, and (c) the median filter using a 3×3 mask.

Table 1. Simulation Results.

Filter	Noise	$\hat{SNR}$	$\hat{MAE}$
Initial	impul-	3.033931	26.466785
MSAM	sive	11.721122	11.004910
SAM	plus	9.271829	13.156524
Median	gaus.	11.187930	12.273333
Initial	pure	9.011253	16.828835
MSAM	gaus-	12.793214	10.185613
SAM	sian	12.466400	10.763560
Median		12.384159	10.654441
Initial	impul-	-0.025914	23.039989
MSAM	sive	14.468263	4.598850
SAM		13.406840	3.082241
Median		12.579622	7.689346

the morphological *SAM* filter outperforms the *SAM* and the median in all cases. This is also verified by comparing Figures 3a,3b and 3c. It is seen that at high corruption levels, the performance of the proposed filter is very satisfactory. This is attributed to three factors: **(i)** the use of large window sizes at homogeneous regions, **(ii)** the anisotropic window increment that allows a higher noise suppression close to edges than the one achieved by the *SAM* filter, and **(iii)** the improved impulse detection mechanism that is now employed. We would like to point out that such a good performance is obtained without any reference image or training procedure and in a single pass. Furthermore, the poor performance of median filters in presence of Gaussian noise is diminished.

The comparison of Figures 3a,3b and 3c reveals that the morphological *SAM* filter achieves a noticeable improvement in visual perception of the filtered images with respect to the quality achieved by the other two filters. This is explained by the fact that the *MSAM* filter achieves to preserve the edges at a high extent, while suppressing the noise in homogeneous regions and removing the impulses very well.

However, a minor disadvantage of the morphological *SAM* filter is its inability to preserve very small details and thin lines. Furthermore, the anisotropic window adaptation procedure requires more computational effort than the isotropic window adaptation used in *SAM* due to erosion and dilation computations.

REFERENCES

[1] R. Bernstein, "Adaptive nonlinear filters for simultaneous removal of different kinds of noise in images", *IEEE Trans. on Circuits and Systems*, vol. CAS-34, pp. 1275–1291, November 1987.

[2] I. Pitas and A.N. Venetsanopoulos, *Nonlinear Digital Filters: Principles and Applications*, Kluwer Academic, Dordrecht, Holland, 1990.

[3] X.Z. Sun and A.N. Venetsanopoulos, "Adaptive schemes for noise filtering and edge detection by use of local statistics", *IEEE Trans. on Circuits and Systems*, vol. CAS-35, no. 1, pp. 57–69, January 1988.

[4] M. Lightstone, E. Abreu, S.K. Mitra, and K. Arakawa, "A new filtering approach for the removal of impulse noise from highly corrupted images", *IEEE Trans. on Image Processing*, vol. 5, no. 6, pp. 1012–1025, June 1996.

[5] R. Sucher, "A recursive nonlinear filter for the removal of impulse noise", in *Proc. of the IEEE Int. Conf. on Image Processing (ICIP'95)*, 1995, pp. 183–186.

[6] M. Gabbouj and I. Tabus, *TUT noisy image database. Technical Report ISBN 951-722-281-5*, Signal Processing Laboratory, Tampere University of Technology, Tampere, Finland, December 1994.